Ab initio investigation of the laser induced desorption of iodine from KI(100)

C. Carbogno,[1] A. Groß,[1] and M. Rohlfing[2]

[1] *Abteilung Theoretische Chemie, Universität Ulm, D-89069 Ulm, Germany*
[2] *Fachbereich Physik, Universität Osnabrück, 49069 Osnabrück, Germany*

(Dated: July 11, 2006)

Based on potential-energy curves that were derived from *ab initio* calculations within the framework of many-body perturbation theory, mixed quantum-classical simulations have been performed to understand the dynamics of the photodesorption process of iodine from KI(100). Dissipation and recoil processes were included by adding a surface oscillator to the *ab initio* potentials. Using this approach, the desorption spectrum and the kinetic energy distribution of the desorbing iodine are reproduced and explained qualitatively.

PACS numbers: 68.43.Bc, 31.15.Qg, 31.50.Gh

I. INTRODUCTION

Due to the evolution of experimental techniques, now allowing a time resolution in the femtosecond regime and even further [1], more and more attention has been given to the dynamics of processes at surfaces. For example, one prototypical photodesorption process is given by the emission of halogene atoms from laser-excited alkali halides, like KI, which has been investigated in a number of experimental and theoretical studies [2–4] . The typical experimental setup consists of a pulsed laser and a time-of-flight measurement of emitted particles. Atom emission from the surface occurs in two different mechanisms. The largest part of the atoms is emitted with a thermal velocity distribution. They are assumed to originate simply from the heating of the surface. In addition to these "thermal" atoms, a second emission mechanism exists in which the chemical bonds of the surface atoms are directly broken by the excitation. Such processes result in much higher kinetic energies than the thermal activation processes. In time-of-flight experiments these fast particles lead to a so-called "hyperthermal" component with much higher velocities. In contrast to the broad velocity distribution of the thermal component, the distribution of the hyperthermal particles is very narrow, indicating a well defined reaction path. In this paper we focus on the dynamics of the system along this path, with a particular emphasis on quantum-dynamical aspects beyond the Born-Oppenheimer approximation. Nevertheless the "thermal" desorption path was inspected as well to gain a complete and in deep understanding of this system.

As far as theory is concerned, dynamical studies based on potentials that were derived from density functional theory (DFT) calculations have been quite successful in reproducing and explaining experimental results [5–7]. In the present case, we encounter two problems forcing us to go beyond that standard approach. First, the potential-energy surfaces (PES) of several quantum-mechanical states involved in the dynamics cross each other. Therefore, the standard procedure of restriction to the Born-Oppenheimer surface (i.e. neglect of electronically non-adiabatic phenomena) is questionable. Secondly, the excited-state PES on which the photodesorption process takes place cannot be obtained from DFT due to the well-known problems of DFT in describing electronic excitations.

Concerning the first of these two difficulties, we have recently implemented a mixed quantum-classical scheme as proposed by Tully [8] in order to treat reaction dynamics at surfaces with electronic transitions [9–13]. This method allows to include non-adiabatic effects and state changes in contrast to ordinary molecular dynamics and furthermore it has no constraints regarding the number of electronic states included and regarding the number of dimensions of the potential-energy surfaces. Additionally the numerical effort is marginal with respect to other techniques (e.g. wave-packet-dynamics). Last but not least the classical treatment of the nuclear coordinates often allows a more intuitive and straightforward insight into the reaction dynamics than multidimensional wave functions may do. Using this methodology, charge transfer processes in molecule-surface scattering [9, 10] and the laser-induced desorption of molecules from surfaces [11, 12] have been modeled.

In order to tackle the second problem of the current situation, i.e. the calculation of the excited-state PES, we employ ab-initio many-body perturbation theory (*GW* method and Bethe-Salpeter equation), which constitutes an extension of DFT towards electronic excitations (electrons, holes, and excitons) [14, 15]. This method has turned out to yield excellent electronic and optical spectra for a large variety of condensed-matter systems.

Using a combination of the two approaches outlined above, we have addressed the laser-induced desorption of iodine from KI(100). Excited-state potentials determined by many-body perturbation theory have been used as an input for mixed quantum-classical simulations. In total, thirteen different electronic states have been taken into account. In addition to the distance of the iodine atom from the surface, a surface oscillator has been considered explicitly in order to model energy transfer processes to the substrate. For the coupling between the electronic states we assumed a physically reasonable dependence on the distance of the iodine atom from the

surface. Using this approach, the experimentally observed desorption spectrum is well-reproduced except for an energy offset, however, we do not find a pronounced bimodality in the kinetic energy destribution of the desorbing atoms, as observed in the experiments.

This paper is structured as follows. In the next section we described both theoretical techniques used in this work, many-body perturbation theory and the mixed quantum-classical algorithm. Then we address the results for the excited-state potential-energy surfaces and discuss the mixed quantum-classical simulations before the paper ends with some conclusions.

II. THEORETICAL METHODS

Here we first discuss the calculation of the potential-energy surfaces by a combination of density-functional theory and ab-initio many-body perturbation theory. Thereafter, we investigate the dynamics of the system within the potential-energy surfaces.

A. Calculation of potential-energy surfaces

The calculations are done within many-body perturbation theory (MBPT) designed for the description of excited electronic states [14, 15]. In all cases we start from a density-functional (DFT) calculation for the electronic ground state.

We employ local-orbital basis sets of Gaussian orbitals, combined with norm-conserving ab-initio pseudopotentials. A generalized gradient approximation (GGA) to the exchange-correlation functional is employed, following Perdew and Wang (PW91) [16]. We note in passing that we have obtained basically the same conclusions from the local-density approximation (LDA). Based on the DFT, quasiparticle (QP) excitations are considered, i.e. single-particle excitation processes in which one additional electron is added (yielding the electron affinity) or removed (corresponding to an ionization process). The calculation of the corresponding QP energies is carried out within the *GW* approximation (GWA) for the electron self energy. In here, electronic exchange and correlation energies are fully contained. Finally, the QP states are used to construct charge-neutral electron-hole excitations, i.e. the excitons. This involves the energies of the QP states and the screened Coulomb interaction between the electron and the hole. Mixing between the various electron-hole configurations is taken into account by solving the Bethe-Salpeter equation, which constitutes the equation of motion of correlated electron-hole pair states.

The ground-state configuration is characterized by a static ionic charge transfer from the cations to the anions, i.e. the iodine ions I^- are in a closed-shell spin-singlet configuration $^1S_0$, and the potassium ions K^+ carry no electrons. Note that at large separation ($z \gtrsim$ 5-10 Å) of the emitted surface anion from the surface this "ground state" is not strictly the ground state but has higher energy than the excited-state configurations discussed below. Nevertheless we use this state as a reference configuration, from which we obtain the other states as "excited states". Formally the "excitation energy" becomes negative at large z.

The calculations are carried out for a spatially isolated cluster geometry rather than for a periodic surface. The latter would require a very large supercell to eliminate artificial interaction between the emitted anion and its replica. Furthermore, a repeated supercell would suffer from artificial electrical long-range dipole-dipole interaction. The dipole occurs between the positively charged vacancy and the negatively charged anion in the ionized "ground-state" configuration. In the excited state, on the other hand, the negative charge is transferred back into the surface vacancy, and no dipole is present. The dipole-dipole contributions to the total energy would therefore be different in the ground state and the excited state, which is very difficult to handle in MBPT.

B. The mixed quantum-classical algorithm

The total Hamiltonian for a system including electronic ($\mathbf{r}$) and nuclear ($\mathbf{R}$) degrees of freedom is

$$\begin{aligned} H &= T_{\mathbf{R}} + T_{\mathbf{r}} + V_{\mathbf{r}} + V_{\mathbf{rR}} + V_{\mathbf{R}} && (1)\\ &= T_{\mathbf{R}} + H_{el}(\mathbf{r},\mathbf{R}) + V_{\mathbf{R}} && (2)\end{aligned}$$

where T denotes the kinetic energy operator and V the respective potentials. All terms depending on the electronic coordinates are grouped together in H_{el} in eq. (2). By expanding the wavefunction in terms of an appropriate orthonormal basis set $\Phi_i(\mathbf{r},\mathbf{R})$,

$$\Psi(\mathbf{r},\mathbf{R},t) = \sum_i c_i(t)\Phi_i(\mathbf{r},\mathbf{R}) \ , \qquad (3)$$

coupling matrix elements V_{ij} between different electronic states can be introduced

$$V_{ij}(\mathbf{R}) = \langle \Phi_i(\mathbf{r},\mathbf{R})|\, H_{el}(\mathbf{r},\mathbf{R})\, |\Phi_j(\mathbf{r},\mathbf{R})\rangle + V_{\mathbf{R}}\delta_{ij} \qquad (4)$$

where the integral is performed with respect to the electronic degrees of freedom. The diagonal elements $V_{ii}(\mathbf{R})$ hereby describe the potential-energy surface for the motion of a nucleus in the electronic state i. Due to the large mass of iodine ($M_{\mathrm{I}} \approx 127$amu) the new Hamiltonian

$$H = T_{\mathbf{R}} + V_{ii}(\mathbf{R}) \qquad (5)$$

can be treated classically. Thus we obtain a set of equations, each one describing the classic trajectory of a nucleus in one specific electronic state:

$$M\frac{d^2}{dt^2}\mathbf{R} = -\nabla_{\mathbf{R}} V_{ii}(\mathbf{R}) \qquad (6)$$

To handle the electronic degrees of freedom the expansion (3) is inserted into the time-dependent Schrödinger equation, leading to following differential equation set for the complex coefficients [8, 13]

$$i\hbar\dot{c}_k = \sum_j c_j(t)\left(V_{kj}(\mathbf{R}(\mathbf{t})) - i\hbar\dot{\mathbf{R}}(\mathbf{t})\cdot\mathbf{d}_{ij}(\mathbf{R}(\mathbf{t}))\right) \ . \quad (7)$$

Here the *non-adiabatic coupling vector*

$$\mathbf{d}_{ij}(\mathbf{R}) = \langle\Phi_i(\mathbf{r},\mathbf{R})|\,\nabla_{\mathbf{R}}\,|\Phi_j(\mathbf{r},\mathbf{R})\rangle \quad (8)$$

is introduced which describes the dependence of the chosen basis set on the nuclear position. The eqs. (6) and (7) are now combined to form a surface hopping method: At each time step the iodine is in exactly *one* electronic state k that determines which potential V_{kk} is used in eq. (6) to compute the classical trajectory. On the other hand, the complete set of equations (7) is integrated to determine the coefficients c_i for *all* electronic states. Hence the density matrix $a_{ij} = c_i^*(t)c_j(t)$, whose diagonal describes the population of each state, can be easily computed. By using random numbers and a switching probability as proposed by Tully [8]

$$P_{k\to j}(t) = \frac{\dot{a}_{jj}(t)}{a_{kk}}\Delta t \ , \quad (9)$$

surface hopping between different electron states k, j is introduced. By using this so called fewest switches algorithm two main constraints can be achieved: The population in each state statistically matches the probabilities given by the a_{ii} and this distribution is achieved with as few surface hops as possible. At the same time, this algorithm allows switches at any point along the trajectory $\mathbf{R}(t)$, even if the potential-energies differ (e. g. $\Delta V = V_{jj}(\mathbf{R}) - V_{kk}(\mathbf{R}) \neq 0$). For switches with $\Delta V \neq 0$, special care has to be taken with respect to energy conservation. If the kinetic energy of the nuclei is smaller than the potential difference ($T_{\mathbf{R}} < \Delta V$), the switches are rejected. If the potential-energy difference is larger than the kinetic energy ($T_{\mathbf{R}} > \Delta V$), the velocities have to be rescaled to fulfill $T^j_{\mathbf{R}} - T^k_{\mathbf{R}} = -\Delta V$. This constraint is not unique because the direction of the velocity adjustment can be chosen freely. Considerations from semi-classical theory suggest to rescale the velocities along the non-adiabatic coupling vector, since forces at state switches usually are parallel to it [17, 18].

The photo-excitation of the iodine ion is treated in a similar manner: For a fixed photon energy E_{photo} and a trajectory in state 1 the potential differences ΔV_i to all other potential-energy surfaces i are computed at each time step. The switching is then modeled by random numbers and the switching probability is given by

$$P_{1\to i}(t) = \frac{1}{\sqrt{\pi\beta}} e^{-\frac{(\Delta V_i - E_{photo})^2}{\beta}}, \quad (10)$$

where β is chosen in accordance with the full width at half maximum $\delta E = 2\sqrt{2\beta\ln 2}$ of the experimental laser pulse. In the case of a switch no energy adjustment is done, i.e. the photo-excitation is assumed to be a Franck-Condon process, but the density matrix elements a_{11}, a_{jj} and a_{1j},a_{j1} have to be permutated.

Please note that in contrast to full quantum mechanics the results of mixed-quantum classical simulations depend on the basis set chosen for the expansion (3) of the wavefunction. In a *diabatic* basis system the diagonal elements of the potential matrix $V_{ij}(\mathbf{R})$ are given from the BSE-GW-DFT calculations (see Sec. II A).

The non-diagonal coupling matrix elements between different states can unfortunately not be provided by DFT calculations. Therefore they have to be chosen as an educated guess. As in previous studies [9–13], we assume the following form of the matrix elements as a function of the distance z from the surface:

$$V_{ij} = \frac{D}{2}\left(1 - \tanh(\alpha(z - z_0))\right) \ . \quad (11)$$

In the absence of any microscopic information we have assumed that the coupling is the same between all states. The parameters have first been guessed and then fine-tuned by comparing simulation and experiment. Best agreement has been obtained for $D = 0.1$ eV, $\alpha = 0.5$ Å^{-1} and $z_0 = 5.0$ Å.

Using an *adiabatic* basis set instead leads to a diagonal matrix V_{ii}, where *non-adiabatic* effects are characterized by the dependence of the electronic wavefunctions on the nuclear coordinates, described by the non-adiabatic coupling vector $\mathbf{d}_{ij}(\mathbf{R})$ (see eq. 8). As a result of the diagonalization, the potential barriers V_{ii} may have changed. This does not affect full quantum mechanics, but leads to differences in the mixed quantum-classical method [8]

Finally we like to comment on the numerical efficiency of our dynamical scheme. In the following we will present the results of one and two-dimensional thirteen-state mixed quantum-classical calculations which means that the coupling between up to 13 different electronic states is included in the simulations. Since both the classical equation of motion as well as the time-dependent Schrödinger equation (7) are integrated simultaneously, the time step has to be rather small due to the small mass of the electrons. The numerical effort is still reasonable due to the extensive use of numerical optimization schemes, with computation times always less than one week on usual workstations for a complete photon energy scan.

The mixed quantum-classical simulations can also easily be carried out in a higher-dimensional framework. For example, the laser-induced desorption of NO from NiO(100) has been studied performing seven-dimensional two-state mixed quantum-classical calculations [11, 12] based on a two-dimensional *ab initio* potential energy surface [19] that has been extended to seven dimensions using a physically reasonable model potential. Hence these simulations are not limited to a small number of dimensions as full quantum dynamical simulations are [7, 20].

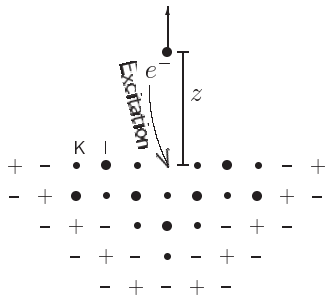

FIG. 1: Structure of the 68-atom cluster configuration used for the simulation of the surface (cross section). Small (large) dots indicate cations (anions). The plus (+) and minus (–) signs indicate the positions of additional point charges, forming an electrostatic background potential. The vertical position (z) of the central surface anion constitutes the generalized coordinate employed throughout the paper.

Furthermore, the collective influence of some electronic excitations could also be included using an optical potential [12, 21]. Thus for example the excitation of electron-hole pairs can be modeled if the details of the excitation distribution are not of interest.

III. RESULTS AND DISCUSSION

A. Excited-state potential-energy surfaces

As discussed in Sec. II A, the calculation of the ground state and excitations is done with a cluster geometry (see Fig. 1).

In our present case, 68 atoms (34 anions and 34 cations) plus 80 point charges are used. We compare the results with those of a 42-atom cluster, showing that with 68 atoms the data is converged to within 0.05 eV (see below). We note in passing that 68 active atoms constitutes the present limit of MBPT calculations of this kind.

The most relevant quantity to characterize the cluster is the vertical position (z) of the emitted anion. During the emission process, two electronic configurations are of particular importance. In the ground-state configuration, the emitted anion is negatively charged with one electron (corresponding to the ionic character of the material). Due to charge neutrality, a positive charge will remain on the cluster, located in the surface vacancy left behind by the emitted atom. From this ground-state configuration, a charge-transfer excitation can be activated in which an electron is transferred back from the negatively charged anion to the positively charged cluster (to be more precise, to the surface vacancy). This excitation is schematically shown in Fig. 1. Note that, neglecting spin-orbit interaction, such charge-transfer excitations can take place at four different energies. The electron can either be taken from the p_x/p_y orbitals of the anion (which are degenerate) or from the p_z orbital, and the transition can occur as a spin iodine-singlet-to-exciton-singlet or iodine-singlet-to-exciton-triplet excitation (the latter ones are three-fold degenerate).This yields 12 excited states for the iodine, in total, with degeneracy of 1, 2, 3, and 6. If the p_x/p_y orbitals are degenerate with the p_z orbital (which is the case at large distance from the surface), the degeneracy becomes 3 (from the singlets) and 9 (from the triplets).

For heavy anions, spin-orbit interaction can be included perturbatively afterwards in the space of these 12 excitations, lifting the partial degeneracy among them. We do this by an additional Hamiltonian $\alpha \cdot \hat{\mathbf{l}}\hat{\mathbf{s}}$ with $\hat{\mathbf{l}}$ and $\hat{\mathbf{s}}$ being the angular momentum operator and spin operator applied to the excess electron on the iodine atom (i.e. the single-particle state which is to become the hole in the excitation). The value of $\alpha = 0.31$ eV reproduces the experimental spin-orbit splitting of 0.93 eV of the neutral iodine atom. Due to the spin-orbit interaction, the degeneracy among the excited states is completely lifted. However, at large distance the p_x/p_y orbitals become degenerate with the p_z orbital, and states can be identified according to the total angular momentum of the neutral iodine I^- atom (1/2 or 3/2, respectively), with degeneracy 2 and 4. In combination with the spin of the electron in the vacancy, we get degeneracies of 4 and 8, i.e. a quadruplet and an octoplet. Since such notation is rather uncommon in the literature, we will instead label these two groups of states as "doublet" and "quadruplet", disregarding the spin state of the vacancy. As can be seen in Fig. 2, this classification holds for all distances.

Fig. 2 displays the total energy of KI(001) as a function of the position z of the emitted anion. The lowest curve denotes the "ground-state" configuration while the upper 12 curves denote the excited states. The solid lines denote the results of the 68-atom cluster configuration, while the dashed curves indicate the data of the 42-atom cluster. Clearly, good agreement is observed between the two sets of calculations, indicating that already the 42-cluster results are well converged with respect to system size. For z=0, our calculated excitation energies of about 5.2-5.4 eV for the I=3/2 surface-exciton states agree well with the experimental data of 5.4 eV measured by Hess et al. [3]. Note that these energies are about 0.2 eV smaller than the onset of the bulk excitons.

As Fig. 2 shows, the ground-state total energy crosses the excited-state total-energy curves. In principle, hybridization and level repulsion would be expected when states with comparable energy interact. This is a general feature of the Bethe-Salpeter equation (also present in configuration-interaction calculations with single excitations): The ground-state configuration and the excited states do not mix, but form separated subspaces in the Hilbert space. This formal description is herein referred to as the expansion in a *diabatic*basis set. The twelve excited-state total-energy curves obtained this way serve as a basis for the dynamics investigated in the next section.

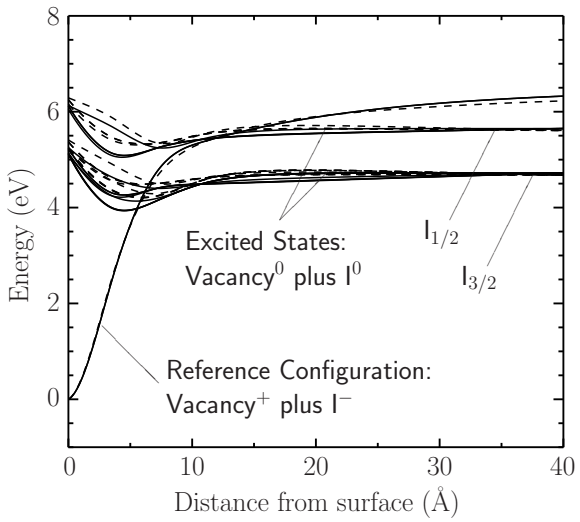

FIG. 2: Total energy of KI(001) as a function of the z position of the emitted iodine anion. Dashed lines refer to the 42-atom cluster geometry while the solid lines denote the 68-atom cluster geometry. The low-energy curve (starting at E=0 at z=0) denotes the electronic ground-state or reference configuration (positively charged vacancy plus negatively charged I^- anion), while the flat upper curves denote the excited states (neutral vacancy plus neutral iodine atom).

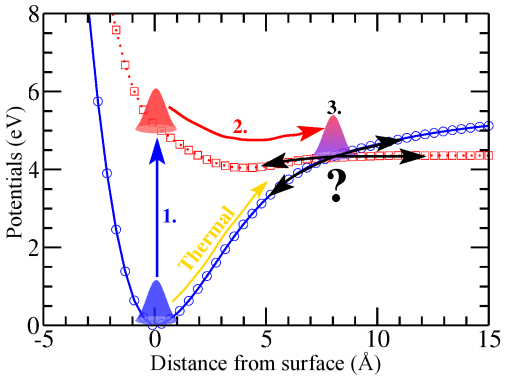

FIG. 3: Illustration of the steps occurring in the laser-induced desorption of iodine from KI(100). Step 1: The ground state I^- ion is excited by a photon. Step 2: Iodine starts to desorb due to the repulsive potential. Step 3: Non-adiabatic effects determine the behavior at the crossing point. The "thermal" desorption path is shown as well.

B. Dynamical modeling of the desorption process

1. *Direct excitation*

As Fig. 3 illustrates, the laser-induced desorption of iodine from potassium exhibits some similarities with the Menzel-Gomer-Readhead scenario of desorption induced by electronic transitions (DIET). The iodine atom first oscillates around the ground state minimum. If hit by a photon with the proper energy, the iodine is excited (*step 1*). This process is modeled by equation (10). Due to the repulsive potential

energy surface the iodine is accelerated away from the surface as shown in *step 2*. However, while in the original DIET scenario the excited and the ground state potential do not cross, for the desorption of I from KI(100) there is a curve crossing (*step 3*). Here we expect non-adiabatic effects to be most influent: State switches and a redistribution of the kinetic energies on the different degrees of freedom may happen.

In our discussion of the dynamical mixed quantum-classical simulations we first focus on the desorption probability of iodine as a function of the incident laser energy. In onedimensional diabatic calculations with a fixed initial total energy k_BT we get square-shaped peaks (see inset in Fig. 4). When switching to a canonical ensemble by choosing random initial positions and Maxwellian distributed velocities with an appropriate thermalization period, the shape of the experimental peak [2] can be well reproduced, as Fig. 4 demonstrates. Still the theoretical peaks are shifted to smaller energies by approximately 0.5 eV, but this is actually not too surprising: While the simulations treat excitons in the surface layer, the excitons in the experiment are probably created in deeper subsurface layers where more energy is required in distorting the crystal lattice; hence the energy needed to create excitons raises typically by some tenths of eV (see Sec. II A and [22]), which would be consistent with our simulations. Unfortunately the desorption probability (○) is unknown for higher laser energies, only the laser absorption (grey area in Fig. 4) has been measured. This distribution is in good agreement with the desorption yield for small kinetic energies, so it should give at least some hints for the behavior at higher frequencies. Apart from the background the laser desorption shows a small subpeak between quadruplet and duplett state and a widely broadened duplett peak showing some substructure. By using an adiabatic basis set this special features could be reproduced as also shown in Fig. 4: The diagonalization of the potential-energy matrix leads to a shift of the potentials in regions with high coupling, especially the energy gap between quadruplet and duplett potentials is filled and the highest duplett state shifts to higher energies.

This produces a desorption spectrum, whose relative peak and subpeak positions can be adjusted by finetuning the parameters in eq. (11). Since the overall peak shift is constant for all spin configurations, we therefore tried to optimize the relative positions of the duplett peak and subpeak.

Experimentally, the state resolved velocity distributions by a combination of REMPI and time-of-flight techniques for the photon energies of a desorption maximum in the quadruplet or duplett state (5.6 eV and 6.4 eV respectively) were also measured [2]. These distributions show a broad thermal peak and a sharp hyperthermal peak whose relative intensity varies depending on the

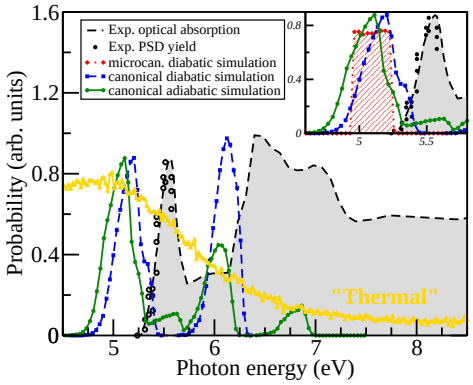

FIG. 4: Desorption probability as function of incident photon energy: Comparison between experimental values [2] and one-dimensional simulations in a diabatic basis set with microcanonical and canonical initial conditions and in an adiabatic basis set with canonical initial conditions. The one-dimensional "thermal" desorption probability for iodine atoms in a diabatic basis set is also shown. The shaded area additionally shows the experimental photon absorption [2].

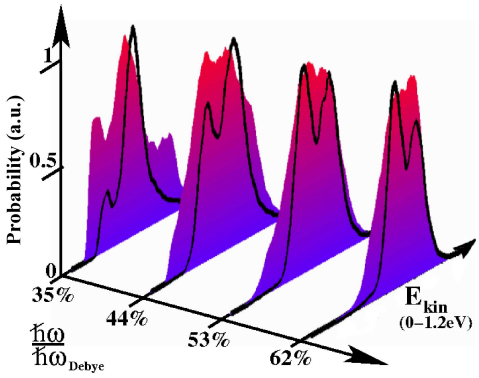

FIG. 5: The kinetic energy distribution for the desorbing iodine in the quadruplet state for different oscillator frequencies: The black line shows the distribution in one, the shaded area the distribution in all eight quadruplet states.

electronic state and the photon energy. In the simulations, photon energies corresponding to the two desorption maxima observed in the experiment were chosen (5.17 eV and 6.1 eV, respectively). Performing one-dimensional mixed quantum-classical simulations of the laser-induced desorption of iodine, the experimentally observed bimodality in the velocity distribution could not be reproduced. This is due to the total energy conservation in the simulation which did not allow to model a thermally accommodated desorption event. In order to include surface recoil and energy dissipation in the simulations, a surface oscillator was introduced by adding a harmonic oscillator potential to the *ab initio* potentials (see eq. (12)), using the mass of potassium ($m_{\mathrm{K}} = 39.1$ amu) and a frequency ω close to the Debye frequency $\hbar\omega_{KI} = 0.114$ eV [23] of KI.

$$V_{2D}(z,x) = V_{1D}(z-x) + m\frac{(\hbar\omega)^2}{2}x^2 \qquad (12)$$

Unfortunately, including a surface oscillator no bimodality was found in the velocity distribution of either all quadruplet or all duplett states. However, the velocity distributions of the individual states (e.g. one out of the $2*4$ quadruplet potential-energy surfaces) exhibit a bimodality which varies depending on the chosen oscillator frequency (see Fig. 5). This feature is caused by the distribution in the oscillator position and velocity during the first excitation (step 1 in Fig. 3). The classical surface oscillator moves either towards the surface or away from it, so that it either slows down or accelerates the desorbing iodine during *step 2* of Fig. 3. Actually the two peaks counterbalance just for oscillator frequencies around 50% of $\hbar\omega_{Debye}$. For smaller frequencies the high energy peak dominates instead, while for higher frequencies the low energy peak does (see Fig. 5). This asymmetry in the kinetic energy distributions is caused by the asymmetry of the ground state potential with respect to its minimum, as can be understood by comparing the (obviously symmetric) harmonic surface oscillator potential with the iodine ground state potential as done in Fig. 6. While the vacuum facing branch of the oscillator is always harder than the ground state, the other, bulk facing branch may be harder, softer or intersect the ground state depending on the chosen frequency as can be seen in Fig. 6. This strongly affects the ground state dynamics of the system, especially the relative amplitudes and turning points of z and x vary and therefore strongly influence the kinetic energy distribution on desorption.

However, this bimodality vanishes when the velocity distribution is summed up over a full spin multiplet (e.g. all of the $2*4$ quadruplet states), as can be seen in Fig. 5, even if each single state shows a bimodality on its own. Due to the potential-energy differences at 0 Å (see Fig. 2), all the single configurations differ in their bimodal kinetic energy distributions, so that the bimodality vanishes when they are added up. This may be another evidence for the creation of the exciton in the deeper layers of the bulk: The potential differences between the different energy surfaces of one spin configuration vanish, i.e. the states become degenerate, when going deeper into the bulk due to the higher symmetry, so that we expect the same bimodal behavior for all states and no cancellation effect when adding them up. Still some serious discrepancies with respect to experiment have to be resolved: While thermal kinetic energies are measured in experiment, all our simulations give kinetic energies of about 0.6 eV. This discrepancy could be resolved by assuming the creation of the exciton in the bulk and a further thermalization of the desorbing iodine while diffusing to the surface which is not taken into account in our calculations. To model this energy transfer processes, a more realistic dissipation mechanism than the relatively simple surface oscillator has to be included into the calculations: The discrepancy between theory and experiment is most probably due to the low dimensionality of the sim-

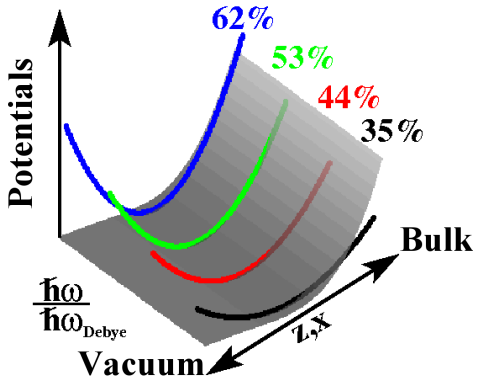

FIG. 6: Comparison of the ground state potential (grey area) at its minimum with the surface oscillator potential for different oscillator frequencies (colored lines). Please note the differences on the bulk facing branches for different oscillation frequencies.

ulations which does not allow to model thermalization processes. Once again this shows how important it is to include more degrees of freedom in this kind of simulations allowing recoil and dissipation mechanisms to act effectively.

2. *"Thermal" excitation*

Due to lack of information about the exact microscopic processes occuring on the surface during laser irradiation, a possible "thermal" desorption has been additionally modelled by initializing the iodine ion in its ground state at 0Å with Maxwellian initial conditions ($T = 470$K in aggreement with experiment [2]). Furthermore, a velocity component $v_{\mathrm{I/SO}}^{\mathrm{nD}}$ derived from E_{photo} is added to the Maxwellian initial velocities of the iodine (and of the surface oscillator SO, respectively, to ensure momentum conservation in the two-dimensional simulations):

$$v_{\mathrm{I}}^{\mathrm{1D}} = \pm\sqrt{\frac{2E_{\mathrm{photo}}}{m_{\mathrm{I}}}} \tag{13}$$

$$v_{\mathrm{I}}^{\mathrm{2D}} = \pm\sqrt{\frac{2E_{\mathrm{photo}}m_{\mathrm{SO}}}{m_{\mathrm{I}}(m_{\mathrm{I}}+m_{\mathrm{SO}})}} \tag{14}$$

$$v_{\mathrm{SO}}^{\mathrm{2D}} = \mp\sqrt{\frac{2E_{\mathrm{photo}}m_{\mathrm{I}}}{m_{\mathrm{SO}}(m_{\mathrm{I}}+m_{\mathrm{SO}})}} \tag{15}$$

Since the ratio of direct to thermal excitations is also unknown, no direct photon excitations to the quadruplet or duplett states were included in these simulations and the desorption process was inspected along the "thermal" pathway schematically shown in Fig. 3. This additional desorption channel is expected to reproduce the Maxwellian kinetic energy distributions found in experiment for the desorbing iodine [2], which it does indeed. In fact the kinetic energy distributions in the simulations are shifted from the starting zero point towards larger values for photon energies higher than the required desorption energy E_{desorb} (4.4eV and 5.3eV for quadruplet and duplett states respectively as shown in Fig. 2). This offset is caused by the excess of energy given to the iodine and the lack of dissipation mechanisms available in such low dimensional simulations, hence a well known artifact of our relative simple "thermal" model.

The simulation results for the desorption probabilities as a function of incident photon energy (see Fig. 4) exhibit some alarming features: Since the energies needed for "thermal" desorption E_{desorb} are smaller than the energies E_{direct} needed for direct excitation (5.2eV and 6.0eV for quadruplet and duplett states respectively as shown in Fig. 2) desorption is observed for much too small photon energies. Furthermore, all trajectories for a photon energy E_{photo} higher than E_{desorb} are able to desorb, which leads to a broad peak with absolute no substructure (see Fig. 4). In addition, the desorption probability for the quadruplet and duplett states falls down to zero for higher photon energies, since the switching probability decreases exponentially for high velocities at the crossing point [24]. Hence the iodine tends to stay in the ionic state and desorb as an ion if energetically possible. Thus an impressive amount of desorbing iodine ions are observed in our simulations for high photon energies, while no evidence for ionic desorption is found in experiment [2]. This ionic desorption is an intrinsic property of the "thermal" pathway and no artifact of our low-dimensional model: When including a surface oscillator the peak in fact shifts towards higher values by a factor of $\sqrt{\frac{m_{\mathrm{I}}+m_{\mathrm{SO}}}{m_{\mathrm{SO}}}} \approx 1.45$ due to the splitting of the photon energy on the different degrees of freedom (see eq. (14) and (15)), but it also gets broader and still falls down to zero and ionic desorption is observed in two-dimensions as well. Therefore the whole "thermal" desorption model seems to be questionable.

IV. CONCLUSION

In this paper we have discussed the dynamics of iodine desorption from KI(001) surfaces. This was done by calculating the ground-state and excited-state potential-energy surfaces within ab-initio many-body perturbation theory, taking the vertical coordinate of the expelled iodine atom as the one dynamical variable of the system. Based on the potential-energy surfaces, we have performed mixed quantum-classical dynamical simulations of the laser-induced desorption of iodine from KI(100) including one atomic coordinate, one surface oscillator coordinate and thirteen different electronic states of the system. Except for an energy set-off, the experimental desorption probability as a function of the photon energy is well-reproduced indicating the reliability of the calculated potential-energy surfaces.

Still the origin of the thermal kinetic energy distribution of the desorbing iodine observed in experiment is unclear: A "thermal" desorption channel seems appealing at first, but such a model leads to ionic desorption which is at variance with the experiment. Therefore we suppose that the thermalization occurs in combination with direct excitation. One main approximation seems to produce the deviations from experiment, namely that we assume that the exciton is created in the surface layer instead of in deeper lying bulk layers. On one hand this affects the energies needed to create excitons and to initiate desorption, on the other hand the diffusion of the excitons to the surface would lead to a thermalization of the iodine atoms by interacting with the bulk's degrees of freedom. Thus the double peak structure observed in the experimental kinetic energy distribution may be caused by the coexistence of high-energy iodine desorption from the surface-layer and thermalized desorption of iodine originating from deeper lying bulk layers.

Acknowledgments

Computational resources were provided by the John-von-Neumann Institut für Computing (NIC), Jülich.

[1] A. Foehlisch, P. Feulner, F. Hennies, F. A, D. Menzel, D. Sanchez-Portal, P. M. Echenique, and W. Wurth, Nature **436**, 373 (2005).
[2] A. Alexandrov, M. Piacentini, N. Zema, A. C. Felici, and T. M. Orlando, Phys. Rev. Lett. **86**, 536 (2001).
[3] see, e.g., W.P. Hess, A.G. Joly, K.M. Beck, M. Henyk, P.V. Sushko, and A.L. Shluger, Surf. Sci. **564**, 62 (2004).
[4] M. Szymonski, J. Kolodziej, Z. Postawa, P. Czuba, and P. Piatkowski, Prog. Surf. Sci. **48**, 83 (1995).
[5] A. Groß, Surf. Sci. Rep. **32**, 291 (1998).
[6] G.-J. Kroes, Prog. Surf. Sci. **60**, 1 (1999).
[7] G.-J. Kroes, A. Groß, E. J. Baerends, M. Scheffler, and D. A. McCormack, Acc. Chem. Res. **35**, 193 (2002).
[8] J. C. Tully, J. Chem. Phys. **93**, 1061 (1990).
[9] C. Bach and A. Groß, Faraday Discuss. **117**, 99 (2000).
[10] C. Bach and A. Groß, J. Chem. Phys. **114**, 6396 (2001).
[11] C. Bach, T. Klüner, and A. Groß, Chem. Phys. Lett. **376**, 424 (2003).
[12] C. Bach, T. Klüner, and A. Groß, Appl. Phys. A **78**, 231 (2004).
[13] C. Bach, C. Carbogno, and A. Groß, Israel J. Chem. **45**, 45 (2005).
[14] M. Rohlfing and S.G. Louie, Phys. Rev. B 62, 4927 (2000).
[15] G. Onida, L. Reining, and A. Rubio, Rev. Mod. Phys. **74**, 601 (2002).
[16] J. P. Perdew *et al.*, Phys. Rev. B **46**, 6671 (1992).
[17] M. F. Herman, J. Chem. Phys. **81**, 754 (1984).
[18] D. F. Coker and L. Xiao, J. Chem. Phys. **102**, 496 (1995).
[19] T. Klüner, H.-J. Freund, J. Freitag, and V. Staemmler, J. Mol. Catal. A **119**, 155 (1997).
[20] A. Groß and M. Scheffler, Phys. Rev. B **57**, 2493 (1998).
[21] D. S. Sholl and J. C. Tully, J. Chem. Phys. **109**, 7702 (1998).
[22] J. Song, R. M. VanGinhoven, L. R. Corrales, and H. Jonsson, Faraday Discuss. **117**, 303 (2000).
[23] W. T. Berg and J. A. Morrison, Proc. Roy. Soc. Ser. A **242** (1957).
[24] C. Zener, Proc. Roy. Soc. London A **137**, 696 (1932).